Pattern-Selective Epitaxial Growth of Twin-Free Pd Nanowires from Supported Nanocrystal Seeds

Youngdong Yoo,[†] Ilsun Yoon,[†] Hyoban Lee,[†] Jihee Ahn,[†] Jae-Pyoung Ahn,[‡] and Bongsoo Kim[†,*]

[†]Department of Chemistry, KAIST, Daejeon 305-701, Korea, and [‡]Advanced Analysis Center, KIST, Seoul 136-791, Korea

ABSTRACT We report that twin-free single-crystalline Pd nanowire (NW) arrays grow epitaxially in a selected pattern on a substrate. Parallel aligned Pd NWs are synthesized on a $SrTiO_3$ (110) substrate in a very high density. On a $SrTiO_3$ (001) substrate, Pd NWs grow horizontally in two perpendicular directions. Vertical Pd NWs are synthesized instead of horizontal NWs when a c-cut sapphire substrate is employed. We reveal that the atomic structure of the substrate surface determines the geometry and orientation of seeds, which in turn direct the growth patterns of the NWs. The interface energy between the NW material and the substrate is also critical in determining the NW growth pattern. Polarization-dependent localized surface plasmon resonance of as-synthesized epitaxial Pd NW arrays is investigated for application as a plasmonic platform.

KEYWORDS: palladium · nanowire · epitaxial growth · single-crystalline · twin-free · localized surface plasmon resonance

Growing single-crystalline metal nanowire (NW) arrays in a well-defined morphology and orientation on a substrate in a large area is important to develop novel functionality in emerging technologies such as plasmonics or spintronics.[1−3] While epitaxial growth would be most effective for this type of patterned growth, few studies have been reported on the epitaxial growth of metal NWs, whereas quite a number of results are reported for that of semiconductor NWs.[4−9] Herein we report the epitaxial growth of twin-free single-crystalline Pd NW arrays in a selected pattern from the supported seed crystals that were formed in a specific morphology on metal oxide substrates.

Pd plays an important role in industrial catalytic reactions, such as hydrogenation/dehydrogenation, automotive exhaust purification, and the oxygen reduction reaction.[10−12] Since the surface atomic structure of the nanomaterial has great influence on its catalytic activity and selectivity, Pd NW arrays epitaxially grown on substrates with well-defined facets can be employed as facet-specific selective catalysts.[13] Furthermore, these epitaxially patterned Pd NW arrays can be utilized in plasmonic applications, such as colorimetric sensing and remote real-time optical sensing of hydrogen.[14,15] Performance of plasmonic devices can be degraded by a rough surface and imperfect crystallinity because of hampered propagation of surface plasmons.[16] Perfect single-crystalline nanoparticles without twins have shown improved performance in molecular sensing using localized surface plasmon resonance (LSPR).[17]

Pd also shows very high sensitivity to hydrogen. Polycrystalline Pd NWs, which have been used for resistance-based detection of hydrogen,[18,19] often have gaps between adjacent grains and show irreversible changes to the measured resistance after exposure to hydrogen. Perfectly single-crystalline Pd NWs would be free of this problem and thus make hydrogen sensors of much improved characteristics.

Various synthetic methods have been developed to grow metal NWs. In a solution phase process, mostly polycrystalline or twinned Pd NWs have been synthesized,[20−25] although nanorods and nanobars with a low aspect ratio have been synthesized in a single-crystalline form.[26,27] A vapor phase process often produces nanostructures of higher crystallinity than the solution-based process because of high substrate temperatures with no participating solvent molecules. Recently, we reported the synthesis of single-crystalline noble metal NWs in a vapor phase process.[28]

Vapor phase methods have been exclusively employed for epitaxial growth of NWs.[4−9] Although epitaxial growth of semiconductor NWs has been successfully accomplished by vapor−liquid−solid process

*Address correspondence to bongsoo@kaist.ac.kr.

Received for review January 25, 2010 and accepted April 27, 2010.

Published online May 10, 2010.
10.1021/nn100151c

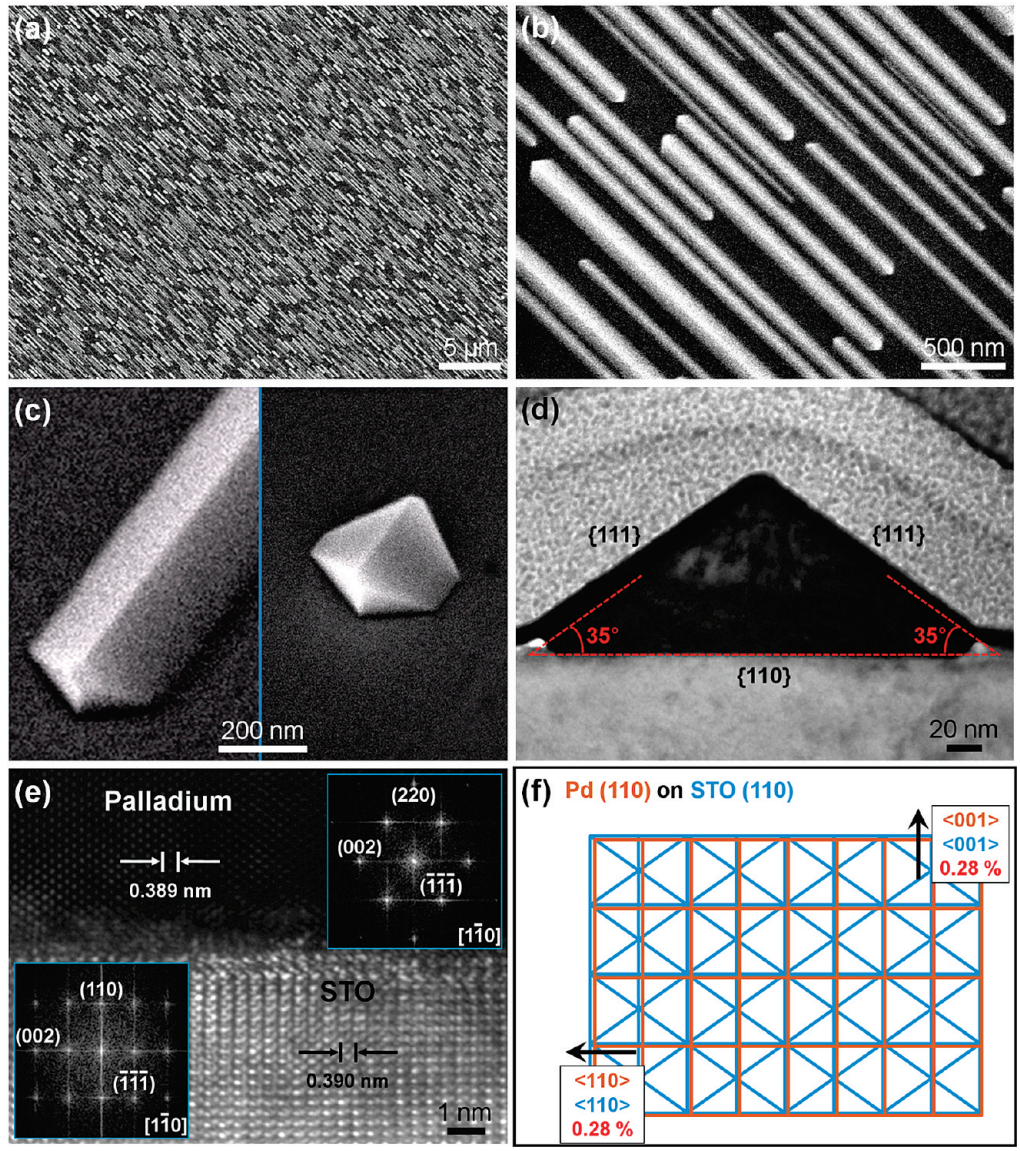

Figure 1. Pd NWs grown horizontally in a single direction on a STO (110) substrate. (a) Top-view SEM image of the NWs. (b) Magnified top-view SEM image of the NWs. (c) Magnified 45° tilted SEM image of the NW and its half-octahedral seed. (d) Cross-sectional TEM image of the Pd NW grown on STO (110). The dark layer covering the Pd NW is a thin layer of Pt, which protects the Pd NW surfaces from ion-beam-induced damage during the focused ion-beam milling. (e) HRTEM image and FFT patterns of the interfacial region between Pd and STO. (f) Schematic of atomic planes at the epitaxial interface between Pd (110) and STO (110).

using metal catalysts,[29] a new method has to be developed for metal NWs because of the absence of appropriate catalysts. Silly *et al.* reported that supported Pd nanocrystals of different morphology were formed on a $SrTiO_3$ (STO) (001) substrate in ultrahigh vacuum depending on the surface reconstruction and the substrate temperature at the time of deposition.[30,31] Pd deposition on other dielectric surfaces has been also reported to produce one-dimensional nanostructures.[32]

By continuously supplying Pd vapor during the growth with optimum experimental parameters, including sufficiently low supersaturation, substrates with good lattice matching, appropriate material flux, and substrate temperature, we have synthesized patterned epitaxial Pd NW arrays that have well-defined morphology in a large area and revealed a detailed growth mechanism. The epitaxial growth pattern of Pd NW arrays is selected by employing substrates of various surface structures such as STO (110), (001), and c-cut sapphire. Furthermore, polarization-dependent LSPR of as-synthesized twin-free parallel Pd NWs is investigated, the result of which suggests a possibility that the as-synthesized parallel Pd NWs can be used as a platform for advanced plasmonic applications.

RESULTS AND DISCUSSION

Horizontal Growth in a Single Direction on a STO (110) Substrate. Figure 1a,b shows top-view scanning electron microscope (SEM) images of Pd NWs grown horizontally in a single direction on a STO (110) sub-

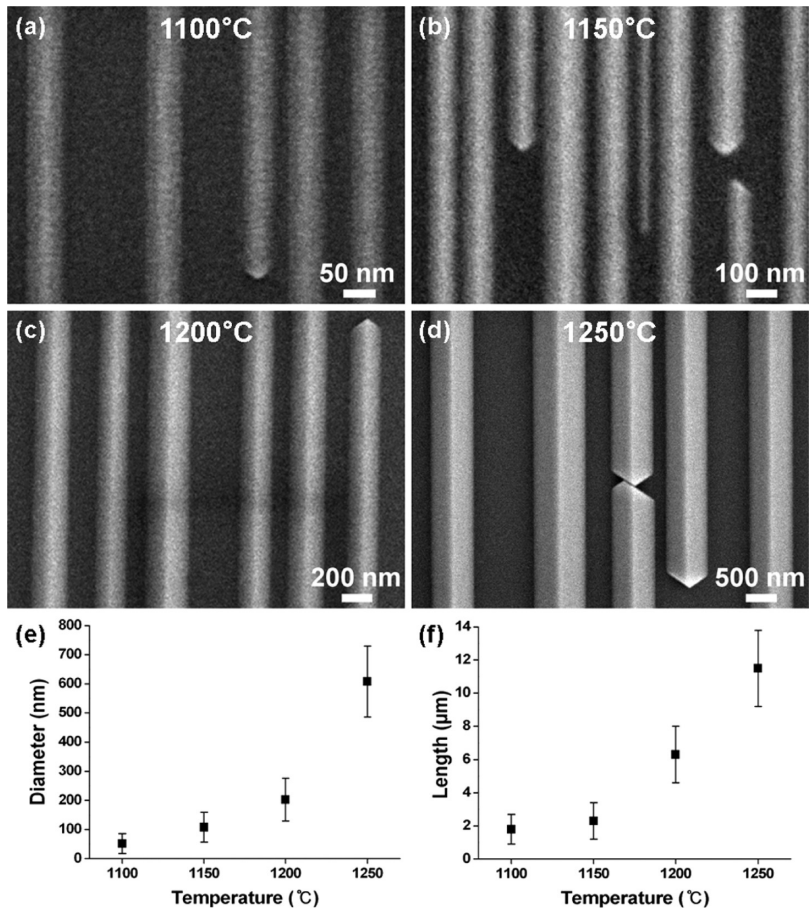

Figure 2. SEM images of Pd NWs grown on the STO (110) substrate at different source temperatures of (a) 1100, (b) 1150, (c) 1200, and (d) 1250 °C. Variation of the (e) diameter and (f) length of NWs as a function of reaction temperature. Each data point represents the average length and diameter of the NWs, and the error bars denote the standard deviation.

strate at a source temperature of 1150 °C. Parallel NWs are synthesized densely on most areas of the substrate. The NW diameter is 108 ± 51 nm (see Supporting Information, Figure S1). The NW is well-faceted and has a shape of an elongated half-octahedron (the left image in Figure 1c). A half-octahedral nanocrystal is also observed on the same substrate (the right image in Figure 1c). The NWs and the half-octahedral nanocrystals have identical orientations, indicating that the NWs grow from half-octahedral nanocrystals. To characterize the growth direction and crystal structure of NWs, cross-sectional transmission electron microscope (TEM) measurement was carried out. The cross-sectional TEM image in Figure 1d shows that the horizontal NW has an isosceles triangular cross section. The angle between the substrate and the side planes of the NW is measured to be 35°, consistent with the angle between the (110) bottom plane and the {111} side planes in an elongated half-octahedron (35.26°). The high-resolution TEM (HRTEM) image and its fast Fourier transform (FFT) patterns (Figure 1e) reveal that the horizontal NW with twin-free single-crystalline nature has a ⟨110⟩ growth direction, {111} side facets, and a (110) bottom plane. Thus, the epitaxial relationship between the horizontal NW and STO is (110) Pd//(110) STO. This characterization of crystal structure of NWs confirms again that as-synthesized NWs are elongated half-octahedrons. Orientation relationship between zone axes of Pd and STO is ⟨110⟩ Pd//⟨110⟩ STO, indicating that Pd NWs grow along a ⟨110⟩ direction of STO. Because there is only one ⟨110⟩ direction on the STO (110) substrate, NWs grow in a single direction on the surface of the substrate. A schematic of atomic planes at the epitaxial interface between Pd and STO in Figure 1f shows that the lattice mismatch between Pd (110) and STO (110) is only 0.28%. Thus, the atomic arrangement of the Pd (110) and STO (110) is quite similar, and the interface energy is highly favorable, leading to horizontal epitaxial NW growth from half-octahedral seeds.

The diameter of the Pd NWs can be controlled by changing the source temperature. At the source temperatures of 1100, 1150, 1200, and 1250 °C and 1 h of reaction time, the average diameters of NWs were 52 ± 34, 108 ± 51, 203 ± 73, and 608 ± 122 nm, respectively (Figure 2). The temperature of the

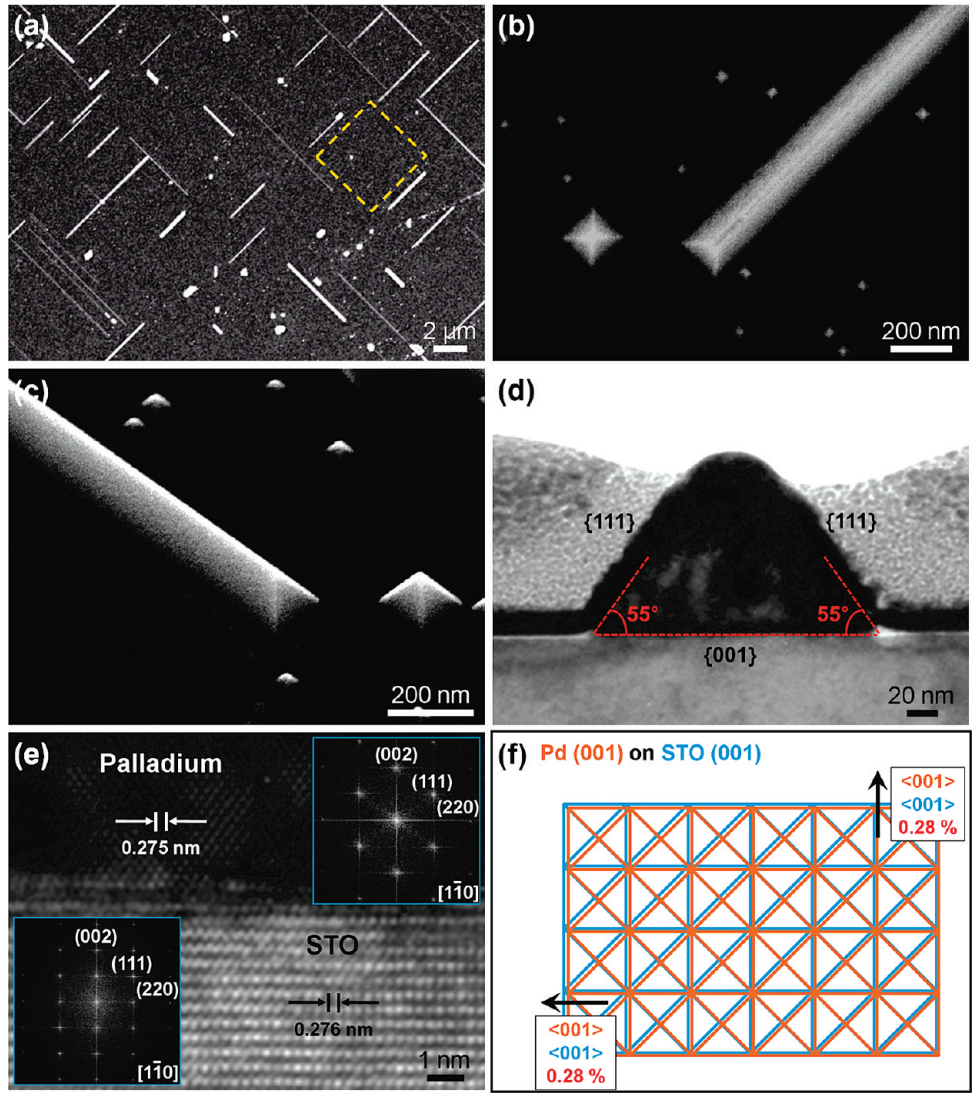

Figure 3. Pd NWs grown horizontally in two perpendicular directions on a STO (001) substrate. (a) Top-view SEM image of the NWs. Magnified (b) top-view and (c) 45° tilted SEM images of the NW and its square pyramidal seed. (d) Cross-sectional TEM image of the Pd NW grown on STO (001). The dark layer covering the Pd NW is a thin layer of Pt, which protects the Pd NW surfaces from ion-beam-induced damage during the focused ion-beam milling. (e) HRTEM image and FFT patterns of the interfacial region between Pd and STO. (f) Schematic of atomic planes at the epitaxial interface between Pd (001) and STO (001).

substrates was maintained at 1000 °C for all experiments. As the source temperature increases, Pd deposition flux increases to induce high driving force for crystal growth, which leads to an increase in the diameter of NWs. The diameter of the NW also increases when the reaction time is increased.

Horizontal Growth in Two Perpendicular Directions on a STO (001) Substrate. Figure 3a shows a SEM image of Pd NWs grown horizontally in two perpendicular directions on a STO (001) substrate at a source temperature of 1150 °C. The NWs are well-faceted and have a shape of an elongated square pyramid (Figure 3b,c). Many square pyramidal seeds are observed in the neighborhood of the NW. Similarity in the geometry and orientation of the square pyramidal seeds to those of the NWs indicates that the NWs grow from square pyramidal seeds. Cross-sectional TEM image shows that the horizontal NWs have an isosceles triangular cross section (Figure 3d). The angle between the substrate and the side plane of the NW is 55°, consistent with the angle between the (001) bottom plane and the {111} side planes in the elongated square pyramid (54.74°). The HRTEM image and its FFT patterns (Figure 3e) reveal that the horizontal NW with twin-free single-crystalline nature has a ⟨110⟩ growth direction, {111} side facets, and a (001) bottom plane. Thus, the epitaxial relationship between the horizontal NWs and STO becomes (001) Pd//(001) STO. These analyses are consistent with the NWs being elongated square pyramids. Orientation relationship between zone axes of Pd and STO is ⟨110⟩ Pd//⟨110⟩ STO, indicating that Pd NWs grow

along a ⟨110⟩ direction of STO. Because the STO (001) substrate has two perpendicular and equivalent ⟨110⟩ directions, NWs grow horizontally in two perpendicular directions on the substrate. A schematic of atomic planes at the epitaxial interfaces between Pd and STO shows that lattice mismatch between Pd (001) and STO (001) is only 0.28%, leading to horizontal epitaxial NW growth from square pyramidal seeds (Figure 3f).

Formation of elongated square pyramidal NWs on the STO (001) substrate that has two equivalent ⟨110⟩ directions can be explained by the following. On the STO substrates having a favorable interfacial energy with Pd, horizontal growth is much faster than vertical growth. Therefore, if a square pyramidal seed grows in both the two equivalent ⟨110⟩ directions on a STO (001) substrate, it would become a square plate with a large (001) top plane. Since the square plate is energetically less favorable than a NW grown by elongation of the square pyramidal seed enclosed by only {111} side facets, the square pyramidal seeds grow along only one of two ⟨110⟩ directions.

STO (001) surfaces can support numerous surface reconstructions that play a key role in the growth of thin films.[30,31,33−36] Silly and Castell reported that a Pd (110) interface is formed on a STO (001)-(2 × 1) surface and a Pd (111) interface or a Pd (001) interface is formed on a STO (001)-*c*(4 × 2) surface depending on the substrate temperature.[30] These reconstructed surfaces were prepared by chemical etching or Ar^+ sputtering. We employed STO substrates as purchased and did not modify them at all. While epitaxial formation of a Pd (001) interface on a STO (001) surface could be well explained by the excellent lattice matching between the two atomic planes, reconstructions of the STO (001) surface could have been possible due to a high reaction temperature (1000 °C). Further STM study would be able to provide detailed information on the surface reconstruction.

When Pd nanocrystals have a (001) interface with the substrate, truncated square pyramids possessing a (001) top plane is the most favorable shape at the thermodynamic equilibrium.[30] Our experimental process, however, is governed by kinetics because adatoms supplied to nanocrystals are continuously deposited and re-evaporated. Since a kinetically controlled process can induce faster growth of {001} facets in Wulff polyhedra,[37] we can obtain square pyramidal nanocrystals enclosed by only {111} side facets under our experimental conditions.

Vertical Growth on a c-Cut Sapphire Substrate. We have obtained vertical Pd NWs instead of horizontal NWs when c-cut sapphire was employed as a substrate (Figure 4a). The average NW diameter is 140 ± 35 nm. The source temperature was 1150 °C in this experiment. A magnified image (tilted 45°) in Figure 4b shows that the Pd NW is an elongated half-octahedron. Figure 4c shows a 45° tilted image of the half-octahedral seed observed on the same substrate. Similarity of the geometry and orientations of half-octahedral seeds to those of vertical NWs suggests that vertical NWs have grown from half-octahedral seeds. The half-octahedral seed grows along the ⟨110⟩ directions because the resulting NWs would be enclosed by the most stable {111} side facets only in this case. NW growth from a half-octahedral seed is thereby confined to either a vertical or horizontal direction. On the c-cut sapphire substrates possessing a sizable lattice mismatch with Pd, NWs grow vertically due to the high interfacial energy between Pd and the substrate (see Supporting Information, Figure S2). From the TEM image of a Pd NW in Figure 4d, the angle between two facets of the NW tip is measured to be 109.5°, consistent with the angle between two {111} top facets of the elongated half-octahedron. HRTEM image of the NW with clear lattice fringes confirms that the NW is single-crystalline with a ⟨110⟩ growth direction (Figure 4e). The lattice spacing of the planes perpendicular to the growth direction is 0.137 nm, agreeing well with the spacing of the (220) planes of a face-centered cubic Pd structure. Selected area electron diffraction (SAED) patterns observed at various zone axes by rotating along the long axis of the NW confirm again the twin-free single-crystalline nature of the NWs (Figure 4f−i).

Growth Mechanism of Pd NWs. Because no catalyst is used and no dislocation is observed in the Pd NWs, vapor−liquid−solid and vapor−solid−solid growth and dislocation-driven growth cannot explain the observed epitaxial growth of Pd NWs.[29,38,39] The growth mechanism can be interpreted instead by the following. The Pd atoms colliding with a substrate gradually form small nanocrystals on the substrate.[40,41] The shape and alignment of the nanocrystals are determined by the surface energies of the nanocrystal facets, the interface energy between the nanocrystal and the substrate, and the surface energy of the substrate.[30] The substrate would thus become a critically important factor to govern the NW growth kinetics. By employing a substrate having different surface atomic structures, we can select the shape and alignment of the seed crystals and control the final alignment and morphology of the NWs.

We have shown that half-octahedral seeds are formed on STO (110) and c-cut sapphire substrates and square pyramidal seeds on a STO (001) substrate. If the seed is half-octahedral or square pyramidal, the resulting NWs would be enclosed by the most stable {111} side facets only when the NWs grow along the ⟨110⟩ directions.[42] Growth to other directions would form less stable facets. Therefore, the NWs grow along the ⟨110⟩ direction to become

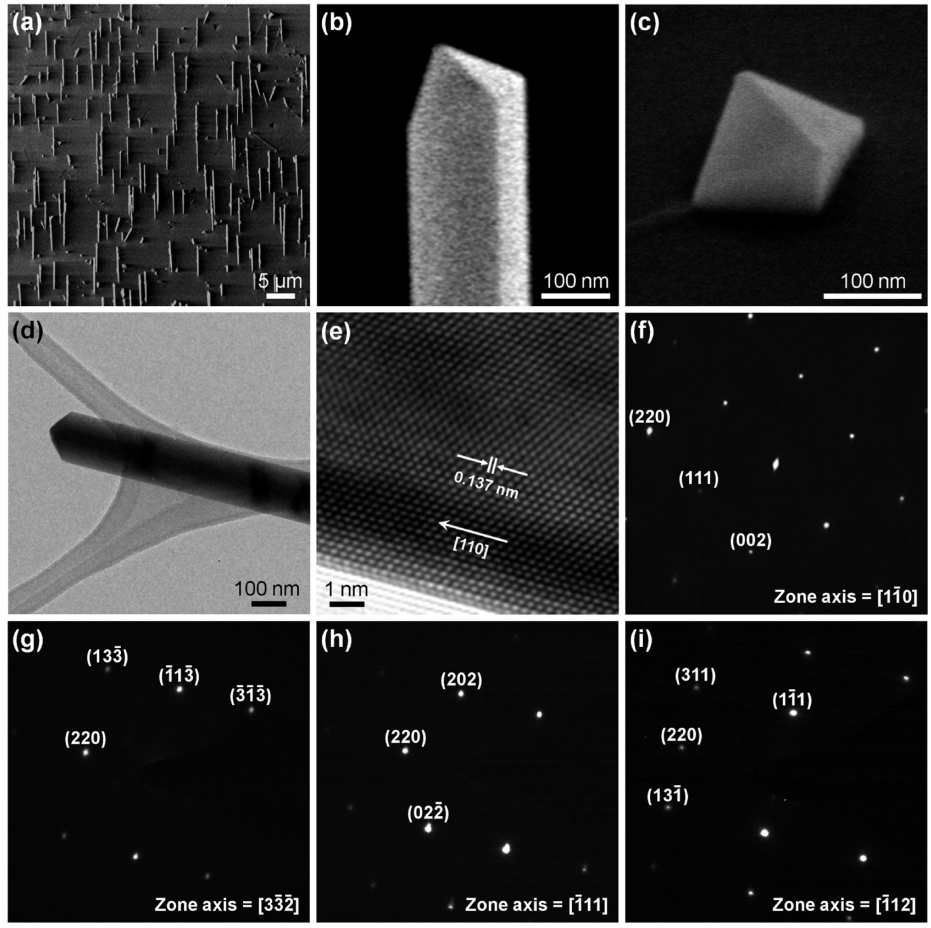

Figure 4. Pd NWs grown vertically on a c-cut sapphire substrate: (a) 45° tilted SEM image of the NWs. Magnified 45° tilted SEM image of (b) the NW and (c) its half-octahedral seed. (d) TEM image of the NW. (e) HRTEM image of the NW. (f−i) SAED patterns observed at various zone axes by rotating along the long axis of the NW.

an elongated half-octahedron or an elongated square pyramid.

Pd atoms approach the seed through two routes, direct collision from the vapor or surface diffusion on a substrate. Pd atoms directly colliding with the seeds from the vapor would contribute to vertical growth because of the angle of collision, whereas Pd atoms approaching the seed by surface diffusion contribute mostly to horizontal growth because they collide against a re-entrant edge of the Pd seed.[43] Thus, growth directions of NWs from the seeds are determined by the competition between vertical and horizontal growth.

On the STO substrates possessing a favorable interfacial energy with Pd, horizontal NWs are formed because horizontal growth is much faster than vertical growth. On the c-cut sapphire substrate possessing a sizable lattice mismatch with Pd, NWs grow vertically because horizontal growth is much slower than vertical growth due to a high interfacial energy between Pd and the substrate.

LSPR Investigation of the Pd NW. Electronic and shape changes can be induced when Pd absorbs hydrogen to form a hydride (PdH_x). Dense and parallel Pd NW arrays can be employed for an effective LSPR sensor that can determine the H_2 concentration by these changes.[14] Bright-field optical microscope image of Pd NWs on a STO (110) substrate shows dense NWs grown in a single direction over a large area (Figure 5a). To investigate LSPR of the Pd NW, we have obtained polarization-dependent dark-field optical microscope images of the same Pd NW arrays (Figure 5b,c). In Figure 5b, the incident light is polarized perpendicularly to the long axis of the NWs. Due to the plasmon resonance of the NW,[44−50] the NWs show bright colors, from red to green, depending on diameters of the NWs. When the incident light is polarized along the long axis of the NWs, no scattered light is observed along the NWs except only at the tips of the NWs (Figure 5c) because plasmon resonance in a longitudinal mode is in the infrared spectral range that could not be observed by our detector, whereas the curvature of the tip makes NWs locally interact with lights.[51,52] Figure 5d,e shows SEM and dark-field optical microscope images of two parallel NWs of different diameters. In Figure 5e, the light was polarized perpendicular to the long axis of the NWs. The SEM and optical images show that LSPR and colors of Pd NWs are strongly correlated with the diam-

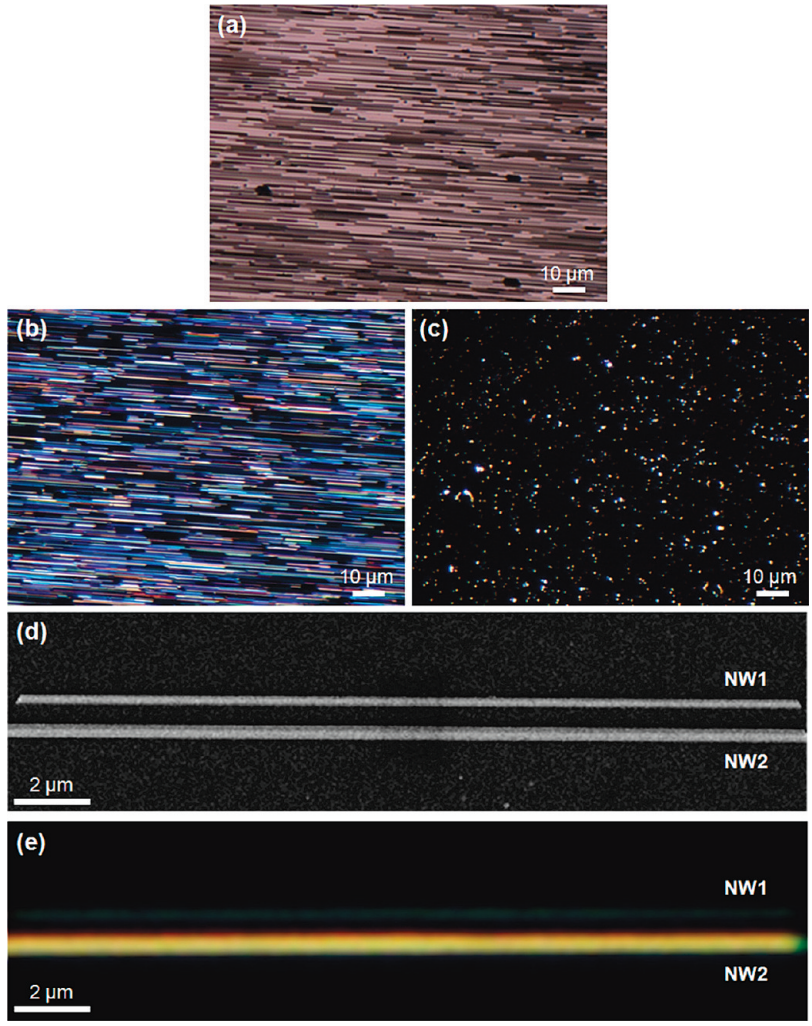

Figure 5. LSPR of Pd NWs grown on a STO (110) substrate. (a) Bright-field optical microscope images of Pd NWs grown horizontally in a single direction on a STO (110) substrate. Polarization-dependent dark-field optical microscope images of the NWs when the incident light is polarized (b) perpendicularly to the long axis of the NWs and (c) along the long axis of the NWs. (d) SEM and (e) dark-field optical microscope images of two parallel NWs of different diameters. The incident light was polarized perpendicularly to the long axis of the NWs.

eter of the NWs and are red-shifted as the diameters of the NWs are increased (see Supporting Information, Figure S3).

CONCLUSION

We have grown twin-free single-crystalline Pd NW arrays epitaxially in a selected pattern on a substrate. On the STO substrates having a favorable interfacial energy with Pd, horizontal Pd NWs are formed. On a c-cut sapphire substrate possessing a high interfacial energy, Pd NWs grow vertically. We have also revealed that the atomic structure of the substrate surface determines the geometry and orientation of seeds, which in turn direct the growth patterns of NWs. We have shown the possibility that the dense arrays of as-synthesized twin-free epitaxial Pd NWs could be used as an advanced plasmonic platform. Further application of these Pd NW arrays as a facet-specific catalytic platform is planned.

METHODS

Synthesis. Single-crystalline Pd NWs were synthesized in a horizontal hot-wall single-zone furnace with a 1 in. diameter inner quartz tube (see Supporting Information, Figure S4). The setup is equipped with pressure and mass flow controllers. The Pd powder (0.02−0.05 g, 99.95%, Sigma-Aldrich) was placed in an alumina boat at the center of a heating zone, and the substrates were placed at a few centimeters downstream from the center of the heating zone. After the quartz tube in the furnace was evacuated to less than 300 mTorr, the carrier Ar gas was supplied through a mass flow controller at a rate of 100 sccm, and the chamber pressure was maintained at 5−15 Torr. The system was purged with Ar gas for 30 min before the start of each reaction to maintain an inert atmosphere. The temperature of the heating zone was raised to the target temperature (1100−1250 °C) at a heating rate of 40 °C/min. Pd powder was heated and evaporated at the center of a heating zone, and the Pd vapor was transported to the lower temperature

region by carrier gas, where Pd NWs were grown on substrates. The distance from the center of the heating zone to the center of the substrate was 5.3, 6.1, 6.9, and 7.7 cm at the source temperature of 1100, 1150, 1200, and 1250 °C, respectively. The temperature of the substrates was maintained at 1000 °C for all experiments. The size of substrate was 5 × 5 mm^2, and the reaction time was between 30 and 60 min. The c-cut sapphire and STO (110) and (001) substrates (MTI Corporation, USA) were cleaned thoroughly by sonication in acetone, ethanol, and water, consecutively, for 15 min each.

Characterization. Field-emission SEM images were taken on a Phillips XL30S. Samples were coated with gold to avoid charging effect during the SEM observation. TEM images, HRTEM images, and SAED patterns were taken on a TECNAI F30 TEM operated at 200 kV. After NWs were dispersed in ethanol, a drop of the solution was put on a holey carbon-coated copper grid for the preparation of TEM analysis. Cross-sectional TEM specimens were prepared by a dual-beam focused ion beam (FEI Nova 600 NanoLab) equipped with a nanomanipulator (Kleindick MM3A). Optical microscope images were taken by using Olympus IX 71 microscope system with an objective (50×, NA = 0.5). A dark-field condenser (up to NA 0.9) was coupled to the microscope system to take dark-field optical microscope images (see Supporting Information, Figure S5). A linear polarizer was coupled with a single slit (width of 3 mm and length of 50 mm) and set in the dark-field condenser. Halogen lamp light (white light) is utilized to illuminate NWs. Polarization direction of the incident light to the NW was controlled by rotating the polarizer in a dark-field condenser.

Acknowledgment. This research was supported by KOSEF through NRL (20090083138), Nano R&D program (20090083221), SRC (2010-0001484), and "Center for Nanostructured Material Technology" under "21st Century Frontier R&D Programs" (2009K000468) of the MEST, Korea.

Supporting Information Available: Diameter distribution of Pd NWs, lattice mismatch of a half-octahedral Pd seed on a c-cut sapphire substrate, LSPR investigation of a single Pd NW, experimental setup used for synthesis of Pd NWs, experimental setup to obtain dark-field optical microscope images, structural model of the half-octahedral and square pyramidal seed, and Pd NWs grown on an Nb-doped STO substrate. This material is available free of charge *via* the Internet at http://pubs.acs.org.

REFERENCES AND NOTES

1. Wolf, S. A.; Awschalom, D. D.; Buhrman, R. A.; Daughton, J. M.; von Molnár, S.; Roukes, M. L.; Chtchelkanova, A. Y.; Treger, D. M. Spintronics: A Spin-Based Electronics Vision for the Future. *Science* **2001**, *294*, 1488–1495.
2. Parkin, S. S. P.; Hayashi, M.; Thomas, L. Magnetic Domain-Wall Racetrack Memory. *Science* **2008**, *320*, 190–194.
3. Kabashin, A. V.; Evans, P.; Pastkovsky, S.; Hendren, W.; Wurtz, G. A.; Atkinson, R.; Pollard, R.; Podolskiy, V. A.; Zayats, A. V. Plasmonic Nanorod Metamaterials for Biosensing. *Nat. Mater.* **2009**, *3*, 867–871.
4. Huang, M. H.; Mao, S.; Feick, H.; Yan, H.; Wu, Y.; Kind, H.; Weber, E.; Russo, R.; Yang, P. Room-Temperature Ultraviolet Nanowire Nanolasers. *Science* **2001**, *292*, 1897–1899.
5. Bakkers, E. P. A. M.; Dam, J. A. V.; Franceschi, S. D.; Kouwenhoven, L. P.; Kaiser, M.; Verheijen, M.; Wondergem, H.; Sluis, P. V. D. Epitaxial Growth of InP Nanowires on Germanium. *Nat. Mater.* **2004**, *3*, 769–773.
6. Sohn, J. I.; Joo, H. J.; Porter, A. E.; Choi, C.-J.; Kim, K.; Kang, D. J.; Welland, M. E. Direct Observation of the Structural Component of the Metal-Insulator Phase Transition and Growth Habits of Epitaxially Grown VO_2 Nanowires. *Nano Lett.* **2007**, *7*, 1570–1574.
7. Hsin, C. L.; He, J. H.; Lee, C. Y.; Wu, W. W.; Yeh, P. H.; Chen, L. J.; Wang, Z. L. Lateral Self-Aligned p-Type In_2O_3 Nanowire Arrays Epitaxially Grown on Si Substrates. *Nano Lett.* **2007**, *7*, 1799–1803.
8. Gao, L.; Woo, R. L.; Liang, B.; Pozuelo, M.; Prikhodko, S.; Jackson, M.; Goel, N.; Hudait, M. K.; Huffaker, D. L.; Goorsky, M. S.; Kodambaka, S.; Hicks, R. F. Self-Catalyzed Epitaxial Growth of Vertical Indium Phosphide Nanowires on Silicon. *Nano Lett.* **2009**, *9*, 2223–2228.
9. Mårtensson, T.; Wagner, J. B.; Hilner, E.; Mikkelsen, A.; Thelander, C.; Stangl, J.; Ohlsson, B. J.; Gustafsson, A.; Lundgren, E.; Samuelson, L.; Seifert, W. Epitaxial Growth of Indium Arsenide Nanowires on Silicon Using Nucleation Templates Formed by Self-Assembled Organic Coatings. *Adv. Mater.* **2007**, *19*, 1801–1806.
10. Thomas, J. M.; Johnson, B. F. G.; Raja, R.; Sankar, G.; Midgley, P. A. High-Performance Nanocatalysts for Single-Step Hydrogenations. *Acc. Chem. Res.* **2003**, *36*, 20–30.
11. Nishihata, Y.; Mizuki, J.; Akao, T.; Tanaka, H.; Uenishi, M.; Kimura, M.; Okamoto, T.; Hamada, N. Self-Regeneration of a Pd-Perovskite Catalyst for Automotive Emissions Control. *Nature* **2002**, *418*, 164–167.
12. Xiao, L.; Zhuang, L.; Liu, Y.; Lu, J.; Abruña, H. D. Activating Pd by Morphology Tailoring for Oxygen Reduction. *J. Am. Chem. Soc.* **2009**, *131*, 602–608.
13. Komanicky, V.; Iddir, H.; Chang, K.-C.; Menzel, A.; Karapetrov, G.; Hennessy, D.; Zapol, P.; You, H. Shape-Dependent Activity of Platinum Array Catalyst. *J. Am. Chem. Soc.* **2009**, *131*, 5732–5733.
14. Langhammer, C.; Zorić, I.; Kasemo, B.; Clemens, B. M. Hydrogen Storage in Pd Nanodisks Characterized with a Novel Nanoplasmonic Sensing Scheme. *Nano Lett.* **2007**, *7*, 3122–3127.
15. Xiong, Y.; McLellan, J. M.; Chen, J.; Yin, Y.; Li, Z.-Y.; Xia, Y. Kinetically Controlled Synthesis of Triangular and Hexagonal Nanoplates of Palladium and Their SPR/SERS Properties. *J. Am. Chem. Soc.* **2005**, *127*, 17118–17127.
16. Nagpal, P.; Lindquist, N. C.; Oh, S.-H.; Norris, D. J. Ultrasmooth Patterned Metals for Plasmonics and Metamaterials. *Science* **2009**, *325*, 594–597.
17. Tang, Y.; Ouyang, M. Tailoring Properties and Functionalities of Metal Nanoparticles through Crystallinity Engineering. *Nat. Mater.* **2007**, *6*, 754–759.
18. Im, Y.; Lee, C.; Vasquez, R. P.; Bangar, M. A.; Myung, N. V.; Menke, E. J.; Penner, R. M.; Yun, M. Investigation of a Single Pd Nanowire for Use as a Hydrogen Sensor. *Small* **2006**, *2*, 356–358.
19. Jeon, K. J.; Lee, J. M.; Lee, E.; Lee, W. Individual Pd Nanowire Hydrogen Sensors Fabricated by Electron-Beam Lithography. *Nanotechnology* **2009**, *20*, 135502.
20. Huang, X.; Zheng, N. One-Pot, High-Yield Synthesis of 5-Fold Twinned Pd Nanowires and Nanorods. *J. Am. Chem. Soc.* **2009**, *131*, 4602–4603.
21. Lim, B.; Jiang, M.; Tao, J.; Camargo, P. H. C.; Zhu, Y.; Xia, Y. Shape-Controlled Synthesis of Pd Nanocrystals in Aqueous Solutions. *Adv. Funct. Mater.* **2009**, *19*, 189–200.
22. Nguyen, K.; Monteverde, M.; Filoramo, A.; Goux-Capes, L.; Lyonnais, S.; Jegou, P.; Viel, P.; Goffman, M.; Bourgoin, J. Synthesis of Thin and Highly Conductive DNA-Based Palladium Nanowires. *Adv. Mater.* **2008**, *20*, 1099–1104.
23. Teng, X.; Han, W. Q.; Ku, W.; Hücker, M. Synthesis of Ultrathin Palladium and Platinum Nanowires and a Study of Their Magnetic Properties. *Angew. Chem., Int. Ed.* **2008**, *47*, 2055–2058.
24. Ranjan, N.; Vinzelberg, H.; Mertig, M. Growing One-Dimensional Metallic Nanowires by Dielectrophoresis. *Small* **2006**, *2*, 1490–1496.
25. Tian, N.; Zhou, Z.; Sun, S. Electrochemical Preparation of Pd Nanorods with High-Index Facets. *Chem. Commun.* **2009**, 1502–1504.
26. Xiong, Y.; Cai, H.; Wiley, B. J.; Wang, J.; Kim, M. J.; Xia, Y. Synthesis and Mechanistic Study of Palladium Nanobars and Nanorods. *J. Am. Chem. Soc.* **2007**, *129*, 3665–3675.
27. Sun, Y.; Zhang, L.; Zhou, H.; Zhu, Y.; Sutter, E.; Ji, Y.; Rafailovich, M. H.; Sokolov, J. C. Seedless and Templateless Synthesis of Rectangular Palladium Nanoparticles. *Chem. Mater.* **2007**, *19*, 2065–2070.
28. Yoo, Y.; Seo, K.; Han, S.; Varadwaj, K. S. K.; Kim, H. Y.; Ryu, J. H.; Lee, H. M.; Ahn, J. P.; Ihee, H.; Kim, B. Steering Epitaxial Alignment of Au, Pd, and AuPd Nanowire Arrays by Atom Flux Change. *Nano Lett.* **2010**, *10*, 432–438.

29. Morales, A. M.; Lieber, C. M. A Laser Ablation Method for the Synthesis of Crystalline Semiconductor Nanowires. *Science* **1998**, *279*, 208–211.
30. Silly, F.; Castell, M. R. Selecting the Shape of Supported Metal Nanocrystals: Pd Huts, Hexagons, or Pyramids on $SrTiO_3$ (001). *Phys. Rev. Lett.* **2005**, *94*, 046103.
31. Silly, F.; Powell, A. C.; Martin, M. G.; Castell, M. R. Growth Shapes of Supported Pd Nanocrystals on $SrTiO_3$(001). *Phys. Rev. B* **2005**, *72*, 165403.
32. Humphrey, D. S.; Cabailh, G.; Pang, C. L.; Muryn, C. A.; Cavill, S. A.; Marchetto, H.; Potenza, A.; Dhesi, S. S.; Thornton, G. Self-Assembled Metallic Nanowires on a Dielectric Support: Pd on Rutile TiO_2(110). *Nano Lett.* **2009**, *9*, 155–159.
33. Newell, D. T.; Harrison, A.; Silly, F.; Castell, M. R. $SrTiO_3$(001)-($\sqrt{5}\times\sqrt{5}$)-*R*26.6° Reconstruction: A Surface Resulting from Phase Separation in a Reducing Environment. *Phys. Rev. B* **2007**, *75*, 205429.
34. Silly, F.; Newell, D. T.; Castell, M. R. $SrTiO_3$(001) Reconstructions: The (2 × 2) to *c*(4 × 4) Transition. *Surf. Sci.* **2006**, *600*, L219–L223.
35. Castell, M. R. Scanning Tunneling Microscopy of Reconstructions on the $SrTiO_3$(001) Surface. *Surf. Sci.* **2002**, *505*, 1–13.
36. Herger, R.; Willmott, P. R.; Bunk, O.; Schlepütz, C. M.; Patterson, B. D. Surface of Strontium Titanate. *Phys. Rev. Lett.* **2007**, *98*, 076102.
37. Baletto, F.; Mottet, C.; Ferrando, R. Molecular Dynamics Simulations of Surface Diffusion and Growth on Silver and Gold Clusters. *Surf. Sci.* **2000**, *446*, 31–45.
38. Wang, Y.; Schmidt, V.; Senz, S.; Gösele, U. Epitaxial Growth of Silicon Nanowires Using an Aluminium Catalyst. *Nat. Nanotechnol.* **2006**, *1*, 186–189.
39. Bierman, M. J.; Lau, Y. K. A.; Kvit, A. V.; Schmitt, A. L.; Jin, S. Dislocation-Driven Nanowire Growth and Eshelby Twist. *Science* **2008**, *320*, 1060–1063.
40. Marks, L. D. Experimental Studies of Small Particle Structures. *Rep. Prog. Phys.* **1994**, *57*, 603–649.
41. Hayashi, T.; Ohno, T.; Yatsuya, S.; Uyeda, R. Formation of Ultrafine Metal Particles by Gas-Evaporation Technique. IV. Crystal Habits of Iron and Fcc Metals, Al, Co, Ni, Cu, Pd, Ag, In, Au and Pb. *Jpn. J. Appl. Phys.* **1977**, *16*, 705–717.
42. Vitos, L.; Ruban, A. V.; Skriver, H. L.; Kollár, J. The Surface Energy of Metals. *Surf. Sci.* **1998**, *411*, 186–202.
43. Choi, K.; Choi, J. W.; Kim, D. Y.; Hwang, N. M. Effect of Coalescence on the Grain Coarsening during Liquid-Phase Sintering of TaC-TiC-Ni Cermets. *Acta Mater.* **2000**, *48*, 3125–3129.
44. Willets, K. A.; Van Duyne, R. P. Localized Surface Plasmon Resonance Spectroscopy and Sensing. *Annu. Rev. Phys. Chem.* **2007**, *58*, 267–297.
45. Mock, J. J.; Oldenburg, S. J.; Smith, D. R.; Schultz, D. A.; Schultz, S. Composite Plasmon Resonant Nanowires. *Nano Lett.* **2002**, *2*, 465–469.
46. Orendorff, C. J.; Sau, T. K.; Murphy, C. J. Shape-Dependent Plasmon-Resonant Gold Nanoparticles. *Small* **2006**, *2*, 636–639.
47. Novo, C.; Funston, A. M.; Mulvaney, P. Direct Observation of Chemical Reactions on Single Gold Nanocrystals Using Surface Plasmon Spectroscopy. *Nat. Nanotechnol.* **2008**, *3*, 598–602.
48. Gunawidjaja, R.; Peleshanko, S.; Ko, H.; Tsukruk, V. V. Bimetallic Nanocobs: Decorating Silver Nanowires with Gold Nanoparticles. *Adv. Mater.* **2008**, *20*, 1544–1549.
49. Pietrobon, B.; McEachran, M.; Kitaev, V. Synthesis of Size-Controlled Faceted Pentagonal Silver Nanorods with Tunable Plasmonic Properties and Self-Assembly of These Nanorods. *ACS Nano* **2009**, *3*, 21–26.
50. Mayer, K. M.; Lee, S.; Liao, H.; Rostro, B. C.; Fuentes, A.; Scully, P. T.; Nehl, C. L.; Hafner, J. H. A Label-Free Immunoassay Based Upon Localized Surface Plasmon Resonance of Gold Nanorods. *ACS Nano* **2008**, *2*, 687–692.
51. Mohanty, P.; Yoon, I.; Kang, T.; Seo, K.; Varadwaj, K. S. K.; Choi, W.; Park, Q.-H.; Ahn, J. P.; Suh, Y. D.; Ihee, H.; Kim, B. Simple Vapor-Phase Synthesis of Single-Crystalline Ag Nanowires and Single-Nanowire Surface-Enhanced Raman Scattering. *J. Am. Chem. Soc.* **2007**, *129*, 9576–9577.
52. Lee, S. J.; Baik, J. M.; Moskovits, M. Polarization-Dependent Surface-Enhanced Raman Scattering from a Silver-Nanoparticle-Decorated Single Silver Nanowire. *Nano Lett.* **2008**, *8*, 3247.